



# The influence of varying Cu doping concentrations on the microstructure, phase evolution and surface wettability of ceramic glazes modified with nano Cu-ZnO

Gokhan Acikbas<sup>1,2</sup> · Nurcan Calis Acikbas<sup>1</sup> · Elif Ubay<sup>3</sup> · Huseyin Karaer<sup>1</sup>

Received: 15 March 2024 / Accepted: 22 April 2024  
© The Author(s) 2024

## Abstract

This study intended to develop nano Cu-doped nano ZnO-modified ceramic glazes. In this scope, nano-sized ZnO and nano Cu powders were incorporated into a commercial glaze composition and then the modified glaze was applied to the surface using the spraying method. The glazed tiles were sintered in a laboratory furnace at 1210°C for 10 min. The surfaces of the sintered samples were analyzed using scanning electron microscopy, X-Ray diffractometer, surface profilometer and contact angle goniometer. The study examined the influence of varying levels of Cu doping on the microstructural evolution and formation of phases, surface roughness, as well as the contact angle. Additionally, wettability conversion experiments were conducted under UV light. As a result, the addition of Cu increased the presence of Willemite crystals and also increasing the quantity and size of Plagioclase crystals. The contact angle of the sintered commercial glaze coated surface was measured to be 51.8°. However, when nano ZnO was added, the contact angle reduced to 44.4°. Likewise, the contact angle of the Cu doped nano ZnO coated surfaces decreased even further to approximately 33°. The inclusion of nano ZnO in commercial glaze resulted in a decrease in the Ra value, while doping Cu led to a modest increase in the Ra value. UV irradiation resulted in a reduction in the contact angles of all surfaces.

**Keywords** Nano Cu-ZnO · Coating · Hydrophilicity · Porcelain tile

## 1 Introduction

In the past twenty years, the ceramics sector for tile production has experienced significant advancements in technology, particularly in production methods and the automation of various stages. However, there is still a need for new products and potential new uses [1]. Porcelain tiles are distinguished from floor and wall tiles due to their hardness, density, increased durability and reduced porosity. Porcelain tiles are categorized into two types: glazed and unglazed. Unglazed porcelain tile exhibits a range of variants (such as double charge, full charge, salt and pepper. etc.) that are created solely through the composition of the tile body, without any additional surface applications (such as engobes, digital ink, or top glazes). Glazed porcelain is a product that has a surface coating applied to it [2]. Upon completion of the firing process, a vitreous substance known as glaze is created on the surface of the product. Glazes play a crucial role in the ceramic tile production process. Traditional glazes typically provide an aesthetic appearance by covering the surface,

---

✉ Gokhan Acikbas  
gokhanacikbas@mersin.edu.tr

Nurcan Calis Acikbas  
nurcan.acikbas@mersin.edu.tr; ncalis@gmail.com

Elif Ubay  
elif.ubay@seranit.com.tr

Huseyin Karaer  
huseyinkaraerkaraer@gmail.com

<sup>1</sup> Department of Metallurgical and Materials Engineering, Mersin University, Mersin 33110, Türkiye

<sup>2</sup> Department of Nanotechnology and Advanced Materials, Mersin University, Mersin, Türkiye

<sup>3</sup> Research and Development Center, Seranit Granite Ceramic Factory, Eskisehir, Türkiye

whereas new generation glazes focus more on functional features. Therefore, in addition to the aesthetic and protective properties of contemporary tile glazes, new generation glazes offer features such as antimicrobial protection, high durability and resistance to wear [3–7]. Enhancing the characteristics of glazes is an ongoing endeavor conducted in numerous research groups. The ceramic tile companies are currently focusing their research on developing novel surfaces that are easy to clean or even self-cleaning. This involves studying various surface structures employing nanoparticles and nanocoatings [8].

One notable property of nano particles is their transparency when applied to a substrate or distributed in a matrix. This characteristic is especially significant for ceramic tiles, as their visual appeal is typically a key factor in marketing. Taking advantage of nanoparticle transparency, the researchers studied various techniques to create a multi-functional surface for ceramic tiles [3–5, 9–15].

Nanomaterials and/or hybrid materials will be essential for designing these novel surfaces. Currently, these innovative materials are rarely utilized in the making ceramic tiles. Hence, it is imperative to devise a novel methodology to effectively choose, manipulate and integrate these components into the ceramic tile surface, with the aim of achieving the desirable characteristics. Various materials, including ceramic tiles, are functionalized commonly with the use of nano  $\text{TiO}_2$  [16–20].

Zinc oxide (ZnO) is often incorporated into ceramic glazes to enhance brightness and inhibit glaze cracking. There are few studies on the use of zinc oxide in ceramic glazes to give various functional surface characteristics [20–23]. On the other hand, hybrid surface morphologies are gaining popularity due to their improved features [24]. Zinc oxide likely exhibits the most diverse range of crystal morphologies compared to other materials [25]. Myint et al. found that the contact angle of ZnO-coated surfaces ranged from  $0^\circ$  to  $151^\circ$ , depending on the morphology and size of the ZnO particles [26]. The diversity of ZnO nanostructures with inherently switchable wettability further encourages their potential use as functional surfaces. According to reported studies, doping nano ZnO particles with various elements or oxides alters their characteristics [27–31]. Moreover, there are a limited number of studies in the literature on Cu-doped ZnO surfaces. In these studies, electronic, optical, photocatalytic and antibacterial properties were investigated [32–37]. There are no studies in the literature on ceramic tiles glazed with nano Cu-doped ZnO particles. Therefore, the study aimed to develop Cu-doped ZnO-modified glaze compositions that had not been evaluated on silicate-based ceramic surfaces before and to characterize the resulting surface properties, namely, microstructure, phase development, surface morphology and contact angle.

## 2 Materials and methods

### 2.1 Materials

In the study, porcelain tile commercial glaze obtained from Seranit Company (Bilecik, Türkiye) and porcelain tiles currently manufactured by Seranit Company was used as ceramic substrates. For the glazing process, ceramic tiles were sized as  $3 \times 3$  cm each. The coating material mixture for the ceramic surface comprises commercial porcelain tile glaze, nano ZnO powder (EgeNanoTek, 20 nm, 99.99% purity) and nano Cu powder (EgeNanoTek, 30–40 nm, 99.95% purity). For the dispersion of the nano ZnO particles, sodium tripolyphosphate (Sigma-Aldrich) was used. The dispersion process of nano Cu particles was carried out in isopropyl alcohol (IP) to reduce the likelihood oxidation.

### 2.2 Characterization of starting nano ZnO and Cu powders

The particle dimensions and shape of the nano ZnO and nano Cu powders utilized in the study were determined using scanning electron microscopy (SEM) (FEG-SEM, FEI, Quanta 650), elemental analysis was carried out by SEM-EDS, and phase analysis using X-ray diffraction (XRD, Rigaku Rint 2000).

### 2.3 Dispersion of nano powders and incorporation into the glaze composition

It is critical to ensure that the suspension to be applied to the surface is prepared homogeneously in order to prevent the development of surface defects or fractures. Prior to further processing, deflocculation was initially performed because of the tendency of nano particles to agglomerate. The STPP dispersant was employed to disperse the nano ZnO powder. The initial stage of dispersing nano ZnO powders involves the utilization of the magnetic mixing technique. 0.2 g of STPP and 7.8 g of nano ZnO powder were blended with 60 ml of distilled water in a 150 ml beaker. The mixture was stirred at a speed of 400 rpm using a magnetic stirrer, at room temperature, for a duration of 30 min. Following magnetic stirring, the mixture was transferred to an ultrasonic bath filled with water, with a height of 30 mm, and treated for a duration of 60 min. In order to inhibit the oxidation of nano Cu particles, they were evenly distributed in isopropyl alcohol (IP). 0.078 g of nano Cu powder were used for 1% Cu doping, 0.39 g for 5% Cu doping, and 0.78 g for 10% Cu doping. These powders were added to 20 ml of IP and stirred using a magnetic stirrer at a rotation speed of 400 rpm for a duration of 30 min. Following magnetic stirring, the suspension was placed in a water-filled ultrasonic

**Fig. 1** Visual representation of the dispersion processes of (a,b) nano ZnO, (c,d) nano Cu and (e) Cu-ZnO mixtures

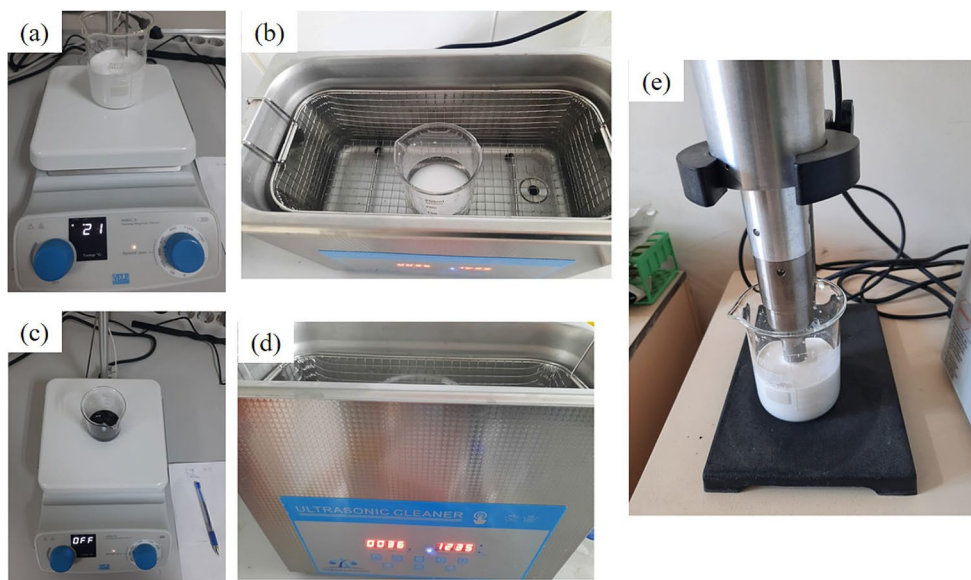


**Table 1** Compositions of nano Cu-ZnO incorporated glazes

Code	Commercial glaze (wt%)	Nano ZnO (wt%)	Nano Cu (wt%)
T-10Z	92.200	7.8	0
T-10Z1C	92.122	7.8	0.078
T-10Z5C	91.810	7.8	0.390
T-10Z10C	91.420	7.8	0.780

bath with a height of 30 mm and left alone for a duration of 60 min. The nano Cu and nano ZnO suspensions were stirred together for 5 min using a magnetic stirrer. Subsequently, the process of sonication was carried out for a duration of 10 min (Fig. 1).

The glaze composition was modified to consist of 40% solids (including porcelain tile glaze, nano ZnO and Cu) and 60% water. The mixture was subsequently blended in a mixer. Following that, the glaze was modified by incorporating nano-ZnO doped with Cu at concentrations of 1%, 5%, and 10% by weight (Table 1). The novel glaze mixture was then subjected to ultrasonic agitation for a duration of 10 min, after which it was prepared for application onto the ceramic surface.

## 2.4 Glazing process

Before glazing, an engobe layer was sprayed onto the ceramic substrates, and novel designed glaze compositions were coated on the engobe surfaces by spraying. Before the glazing process, the glaze's viscosity was adjusted to the desired fluidity by adding STPP and water, and the glaze liter weight was set to  $1350 \pm 27$  g/L and the Lehman viscosity to  $12 \pm 2$  s. A single layer of glaze was applied to the surface, which was then dried in an oven at  $110$  °C for 30 min.

## 2.5 Firing

The sintering process was carried out at a temperature of  $1210$  °C for a duration of 10 min in a laboratory furnace.

## 2.6 X-ray diffraction (XRD) for phase analysis

The examination of the sintered surfaces and starting powders was conducted using Cu-K $\alpha$  radiation with the Rigaku Rint 2000 XRD equipment. The analysis was performed at a scanning speed of 2 degrees per minute within the  $2\theta$  range of 20 to 40 degrees.

## 2.7 Microstructure analysis with scanning electron microscopy (SEM)

Prior to SEM analysis, ceramic surfaces were coated with gold, a highly conductive material, in a vacuum environment to ensure conductivity and hence prevent electron charging on the surface. Scanning electron microscopy (FEG-SEM, FEI, Quanta 650), secondary electron (SE) detector, back scattered electron detector (BSE), and energy dispersive X-ray spectroscopy (EDS) were used to analyze the microstructure of the glazed surfaces. The EDS mapping was employed to ascertain the distribution of nano particles on the surface. The measurement of coating thickness was determined using BSE imaging.

## 2.8 Surface contact angle measurement

Contact angle and surface free energy (SFE) were determined using a drop shape analyzer (Kruss, DSA-25) using water and diiodomethane as the liquids having known

surface tensions in air [12]. The SFE calculations were performed using Young's equation and a two-component model derived from Fowkes and Owens, Wendt, Rabel, and Kaelble (OWRK methodology) [38–40].

## 2.9 Surface roughness measurement

The roughness of the produced surfaces was measured using the Mitutoyo SJ-410 surface profilometer.

## 2.10 Wettability conversion experiments under UV light

Wettability conversion experiments were conducted with a commercial UV lamp that had 8 W dual lamps, providing an intensity of around  $1.0 \text{ mW/cm}^2$  [26]. Contact angle measurements were conducted on the surfaces that were exposed to UV light for 60 min.

# 3 Results and discussion

## 3.1 Characterization of nano powders

SEM investigations revealed that nano Cu particles were spherical in shape and ranged in size from 40 to 600 nm. EDS study revealed that they contained 99.03 wt% Cu and a very little quantity (0.97%) of oxygen (Fig. 2a, b).

XRD study confirmed that it was only in the copper phase (Fig. 2c).

The nano ZnO powders appeared to be rod-shaped, with a width ranging from 60 to 100 nm and a size of around 500 nm. EDS study revealed that the particles only consisted of zinc and oxygen (Fig. 3a,b). XRD analysis showed that it was in the zincite phase (Fig. 3c).

## 3.2 Distribution of nano powders on the surface

The EDS mapping method was used to determine the distribution of nano Zn and nano Cu powders on the sample surface coded T-10Z1C (Fig. 4). When the resulting image was examined, it showed that Zn and Cu elements were uniformly distributed throughout the surface. The dispersion of the nano particles was efficient.

## 3.3 Determination of glaze coating thickness

Glaze coating thickness was determined with the SEM-BSE detector. Figure 5 shows a representative SEM-BSE image from the cross section of the sample designated T-10Z. Engobe thickness ranged from 40 to 50  $\mu\text{m}$ , whereas glaze thickness was approximately 130  $\mu\text{m}$ .

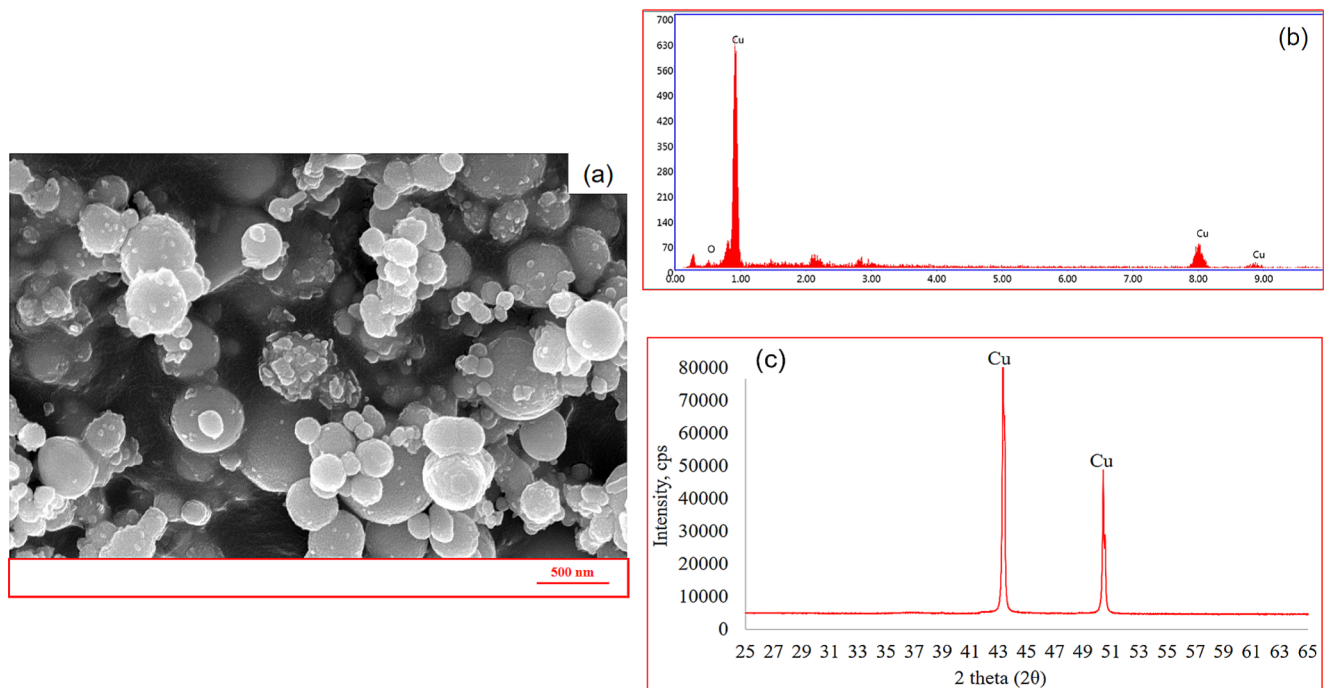


**Fig. 2** (a) Representative microstructural image of nano Cu powder taken with SEM-SE detector (100kx), (b) EDS analysis spectrum, (c) XRD graph



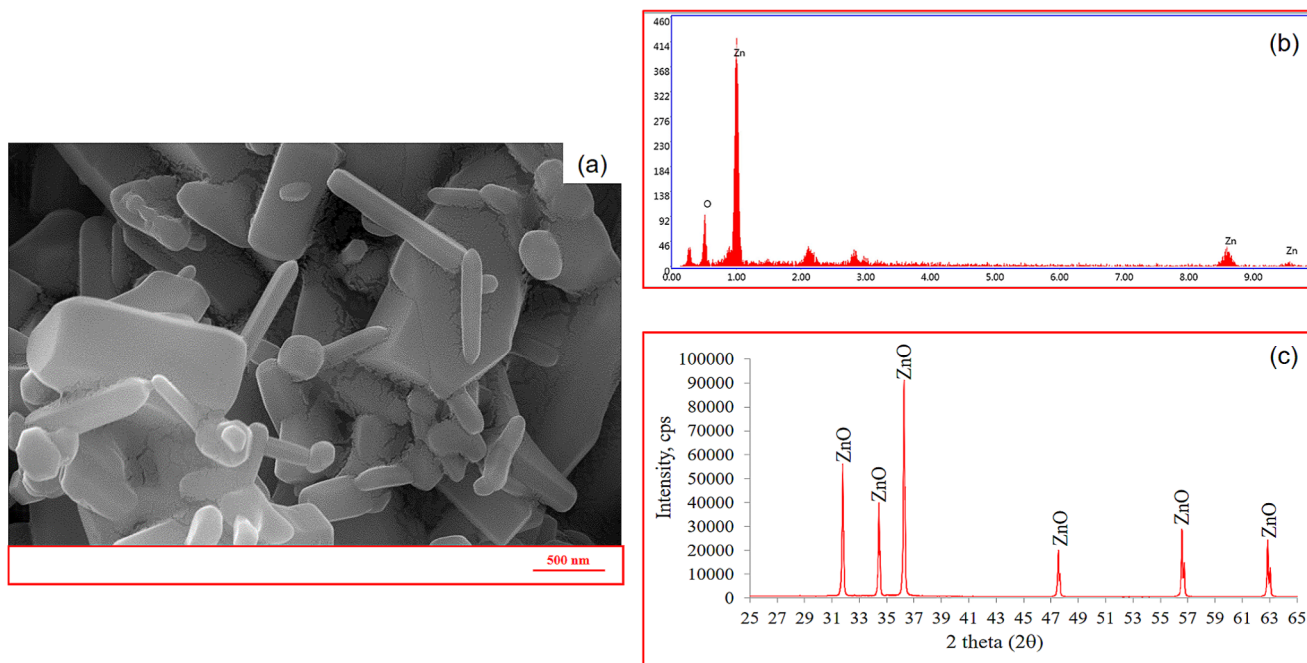
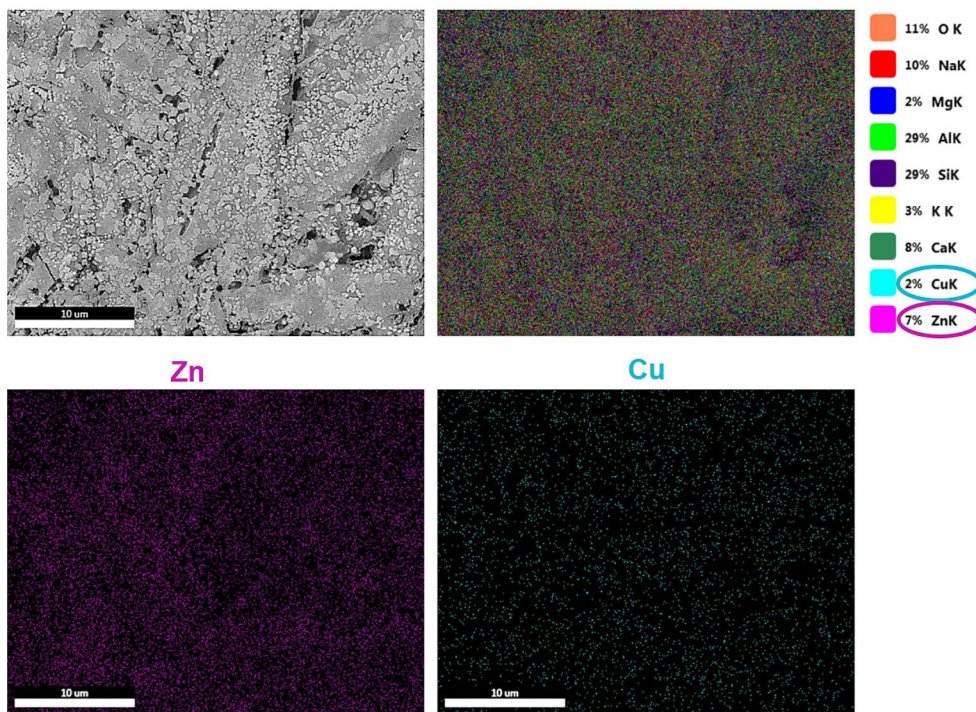


Fig. 3 (a) Representative SEM-SE image of nano ZnO powder (100kx). (b) EDS analysis spectrum, (c) XRD graph

Fig. 4 SEM-EDS mapping image taken from the 1% Cu doped ZnO modified glaze



### 3.4 Effect of Cu doping on phase development

Figure 6 displays the phase development graph of sintered samples based on their composition. The primary phase identified after the incorporation of 10% nano ZnO in the commercial porcelain tile glaze was Willemite ( $Zn_2SiO_4$ ). The majority of the nano ZnO powder underwent a reaction

with  $SiO_2$  in the mixture, resulting in the formation of the  $Zn_2SiO_4$  phase. The JPDS cards indicate that the most intense peak of the Willemite phase (I: 97.61) occurs at 33.93 degrees, the second most intense peak (I: 73.52) at 25.49 degrees, the third most intense peak (I: 44.57) at 31.44 degrees, the fourth intense peak (I: 28.36) at 38.72 degrees, and the fifth intense peak (I: 28.29) at 22.03 degrees. The

**Fig. 5** Representative SEM-BSE image taken from the cross section of the sample coded T-10Z

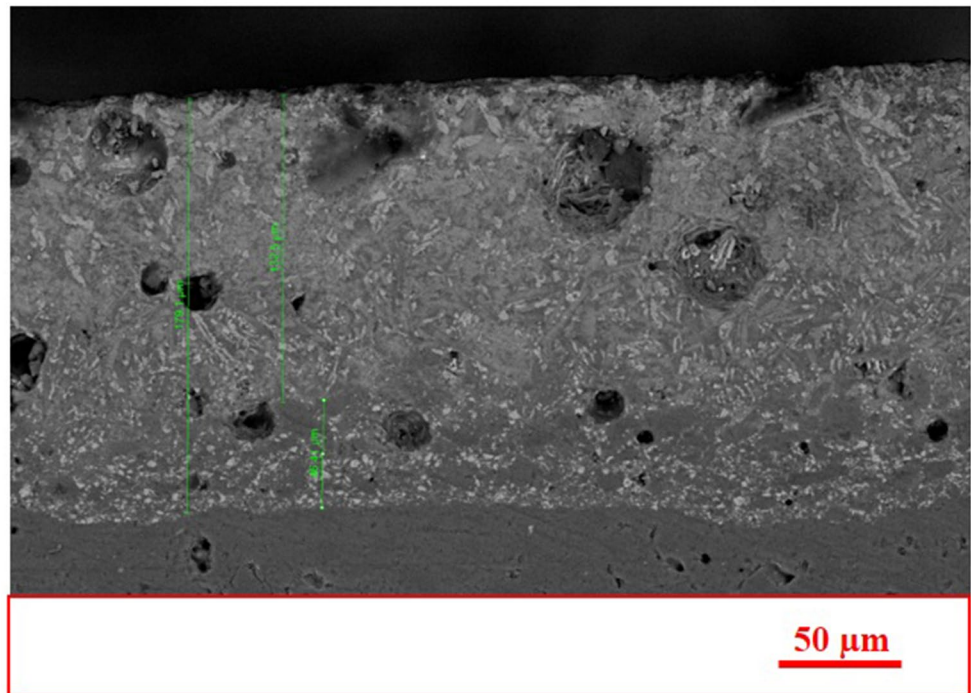
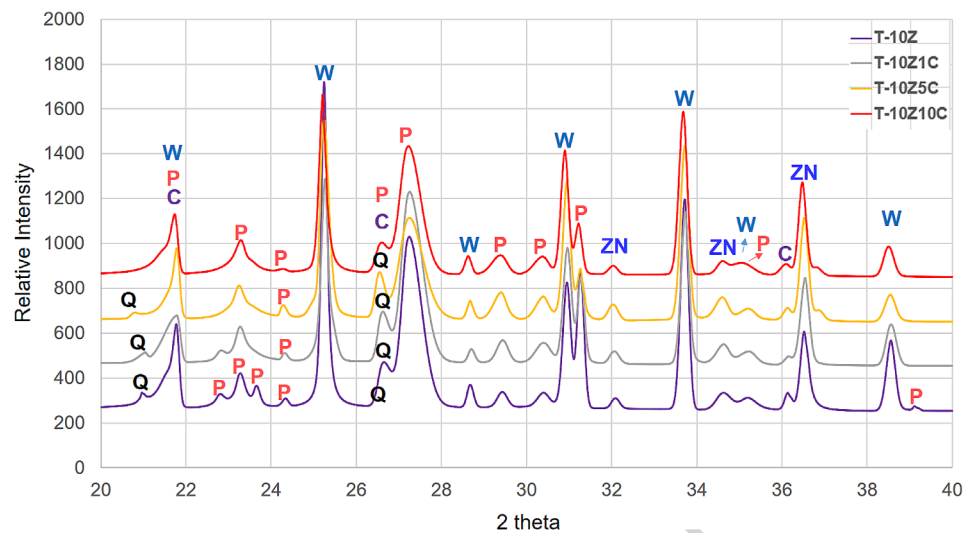


**Fig. 6** XRD graphics of Cu doped ZnO modified glazed surfaces (W: Willemite, ZN: Zincite. P: Plagioclase, Q: Quartz, C: Cristobalite)



most prominent Willemite peak was detected at an angle of 25.49 degrees 2 theta due to its orientation. The stability of the zincite (ZnO) phase indicates that some nano ZnO particles remain inert and do not undergo reactions. The zincite phase exhibits its most intense peak at 36.24°, the second most intense peak at 31.76°, and the third most intense peak at 34.42°. The third noteworthy peak is the Plagioclase phase, which is an aluminosilicate mineral dominated by feldspar and formed as a devitrification result. Quartz and Cristobalite phases are also present. Because only a little amount (less than 1 wt%) of nano copper powder was used in the study, phase development containing the Cu element was not detectable.

Figure 7 displays graphs illustrating the influence of Cu doping on W/P, P/W, W/ZN, and ZN/W phase ratios. The ratio of the highest peak heights of Willemite crystals (at  $2\theta = 33.93^\circ$ ) to Zincite crystals (at  $2\theta = 36.24^\circ$ ) in the XRD patterns is denoted as W/ZN. On the other hand, the ratio of the second most intense peak of Willemite crystals (at  $2\theta = 25.49^\circ$ ) to Plagioclase crystals (at  $2\theta = 27.3^\circ$ ) in the XRD patterns is denoted as W/P.

The T10Z sample has a W/P ratio of 1.83 and a W/ZN ratio of 2.45. By adding 1% Cu, the W/P ratio reduced to 1.07 and the W/ZN ratio decreased to 1.66. The Cu doping promoted the formation of Plagioclase crystals, and the highest P/W ratio (0.94) was achieved with 1% Cu doping.

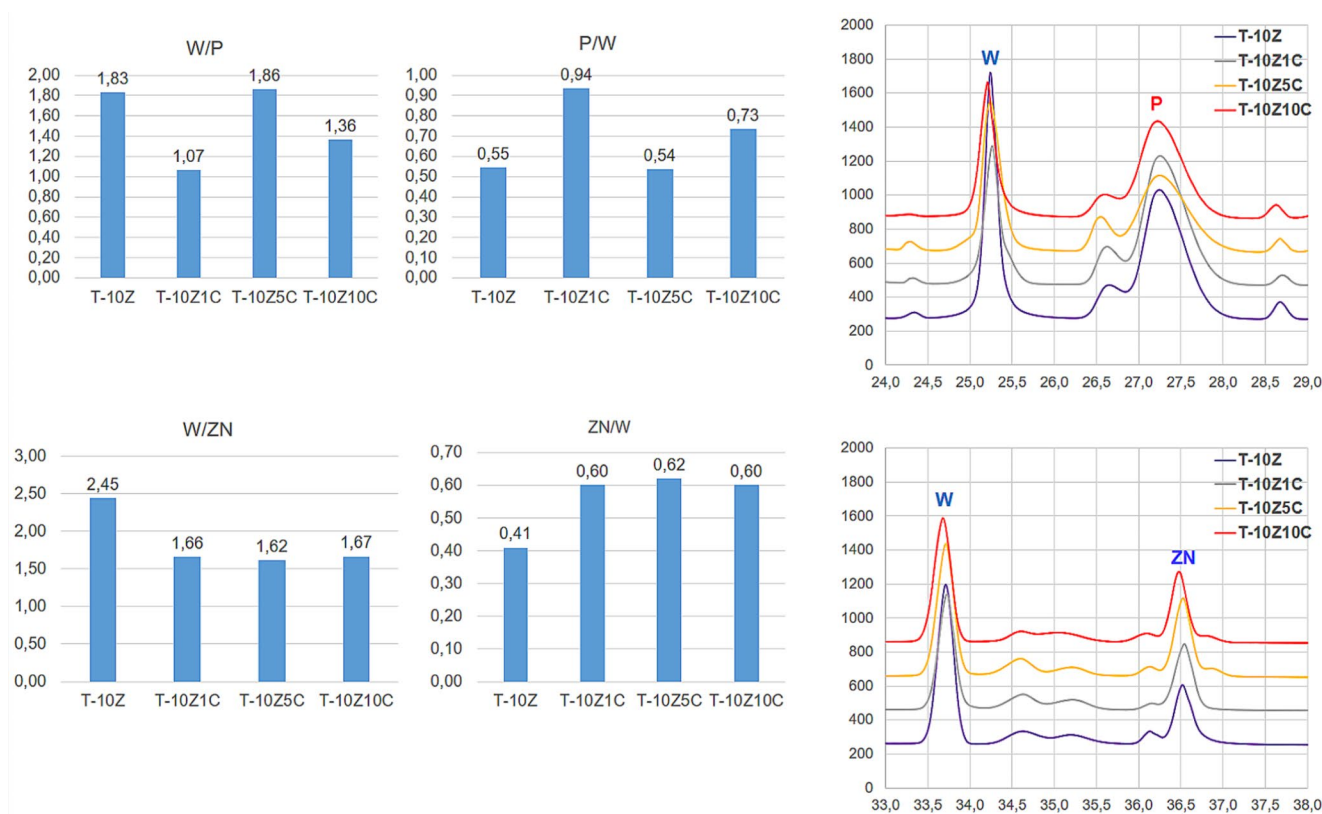


**Fig. 7** Effect of Cu doping on W/P, P/W, W/ZN and ZN/W phase ratios on sintered surfaces

The 5% Cu doping increased the visibility of willemite crystals while decreasing the P/W ratio (0.54) substantially. The XRD graphs and SEM images verified the morphological and quantitative alterations in willemite crystals. At a Cu ratio of 5%, the W/P ratio is 1.86 and the W/ZN ratio is 1.62. With 10% Cu doping, the W/P ratio becomes 1.36 and the W/ZN ratio is 1.67. ZN content rises with copper doping, while the ratio of W to ZN remains consistent across all levels of copper doping. The surface doped with 5% Cu had a maximum W/P ratio of 1.86, the surface doped with 1% Cu had the highest P/W ratio of 0.94, and the nano ZnO doped surface without Cu had the highest W/ZN ratio of 2.45.

The ZN/W ratio rose with the addition of Cu. While the amount of Zincite phase formation on the nano ZnO added surface was low (ZN/W: 0.41), the amount of Zincite phase increased with Cu doping (Z/W: 0.60–0.62). The ZN/W ratios at 1, 5, and 10 Cu doping rates are similar (0.6 and 0.62).

The W/P ratio varies between 1.07 and 1.86. With 1% Cu doping, the W/P ratio dropped from 1.83 to 1.07, rose to 1.86 with 5% Cu doping, and reduced to 1.36 with 10% Cu doping. Increasing the Cu concentration from 1 to 5% provided the Willemite phase more prominent than the Plagioclase phase.

### 3.5 Effect of Cu doping on microstructural evolution

Figure 8 shows SEM-BSE images obtained at various magnifications (20kx, 50kx and 100kx) of sintered surfaces with nano ZnO added and Cu doped at varying contents. Upon evaluation of SEM images. Plagioclase crystals/nuclei are visible as little spherical grains on the Willemite grains, and the gray patches at the bottom represent Willemite crystallization. It was noted that Willemite crystals became more noticeable with Cu doping, and there was an increase in both the quantity and size of Plagioclase crystals. SEM images indicated that Willemite crystals became more evident when 5 and 10% Cu were incorporated.

Cu doping enhanced the formation of Plagioclase crystals, and 1% Cu doping resulted in the highest P/W ratio (0.94). The 5% Cu doping boosted the visibility of Willemite crystals while significantly lowering the P/W ratio (0.54). The XRD graphs and SEM photos confirmed the morphological and quantitative changes in Willemite crystals. Increasing the amount of copper doping to 10% results in a reduction in the size of Plagioclase crystals and an increase in their quantity, leading to a corresponding increase in the P/W ratio (0.73).



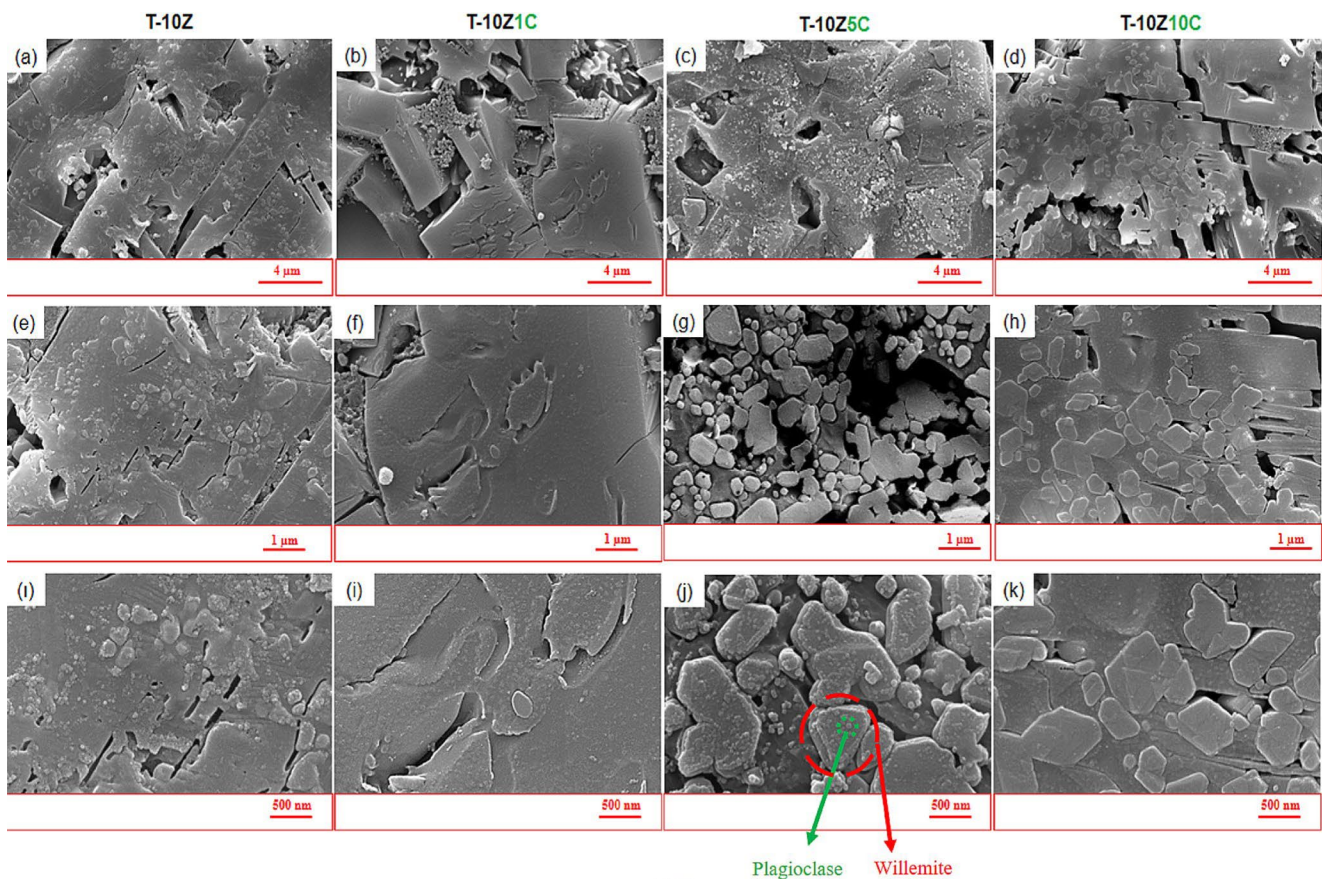


**Fig. 8** Representative SEM-BSE images at various magnifications (20kx, 50kx and 100kx) of sintered surfaces with nano ZnO added and varying content Cu doped glazed surfaces

**Table 2** The contact angle and surface energy values of the created surfaces based on composition

	Contact angle (°)	Specific surface energy (mJ/m <sup>2</sup> )	Ra (μm)	W/ZN	W/P
T-10Z	44.4	85.7	1.164	2.45	1.83
T-10Z1C	33.4	91.9	1.319	1.66	1.07
T-10Z5C	33.8	92.2	1.454	1.62	1.86
T-10Z10C	33.6	93.1	1.582	1.67	1.36

### 3.6 Effect of Cu doping on contact angle and surface roughness

The contact angles and specific surface energy of the surfaces with different Cu content were measured and the obtained results are presented in Table 2. Upon evaluation of the surfaces based on physical appearance, it is observed that the glaze fully melts and covers the surface without any porosity at the firing temperature. The phenomenon occurred because the copper-doped zinc modified glaze vitrified sufficiently to provide a glassy surface at the sintering temperature.

All surfaces have similar surface roughness values, ranging from 1.16 to 1.58 μm. Specific surface energies range from 85.7 to 93.1 mJ/m<sup>2</sup>, with contact angles ranging from 33.4° to 44.4°. The reduction in the contact angle from 44° to 33° by doping Cu represented an alteration in the surface chemistry towards a more hydrophilic state. The surface free energies of the ceramic tiles modified with Cu-doped ZnO were strongly related to the contact angles, as shown in the graph in Fig. 9. The data showed that surfaces with higher surface energy had lower contact angles. As demonstrated through practical evidence, increasing the surface free energy was crucial for creating a superhydrophilic surface in conformity with the principles of theory. Chemically hydrophilic surface can transition to hydrophobic or super hydrophobic due to changes in surface morphology when the surface free energy is greater than the solid surface energy. The hydrophilic effect remained nearly constant with Cu doping as there was no alteration in surface roughness values.

Cu doping resulted in a relatively higher surface roughness value and a lower contact angle (Fig. 10). Because the key elements influencing the contact angle are surface roughness and surface chemistry (energy), the generated



**Fig. 9** Relationship between contact angle and surface free energy of nano copper-doped zinc oxide modified ceramic tile surface

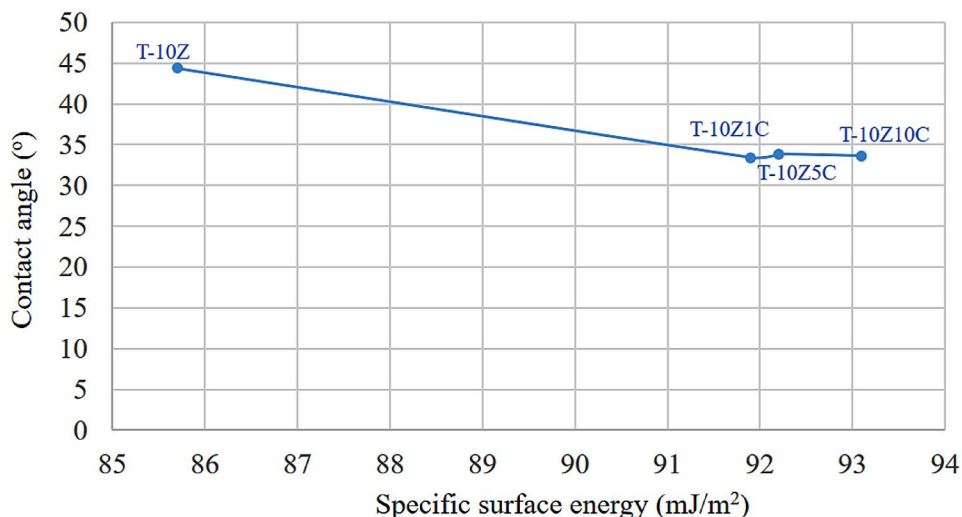
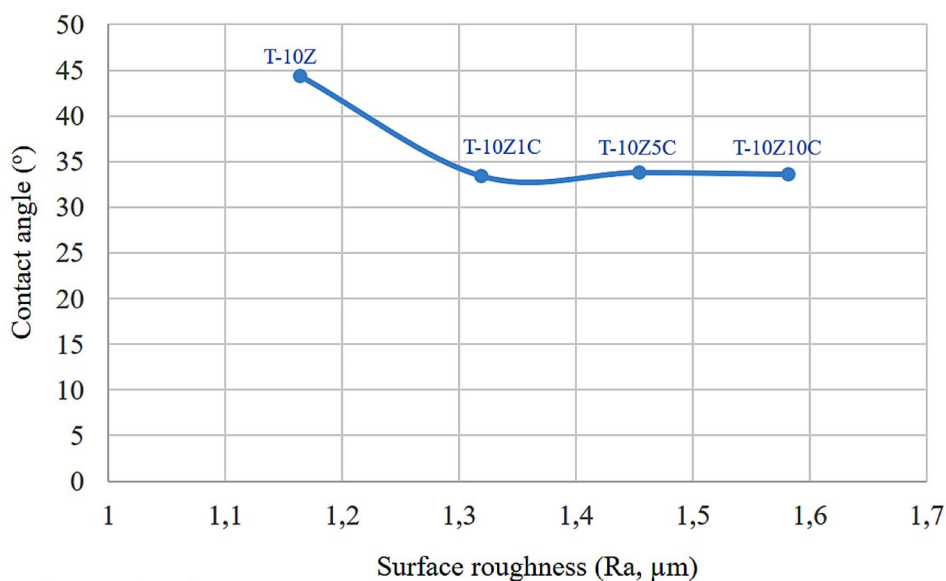


**Fig. 10** Contact angle of the nano Cu doped ZnO modified ceramic tile surface versus surface roughness parameter



surfaces have almost similar surface roughness values and surface energies, and all surfaces are hydrophilic. The predominant phases on all surfaces are Willemite, followed by Plagioclase and Zincite. The microstructural difference is the size and quantity of the Plagioclase and Willemite crystals. The higher quantity of the Willemite phase compared to the zincite and Plagioclase phases could have led to an increased contact angle. In terms of phase relation as the ZN/W ratio increased, the contact angle dropped.

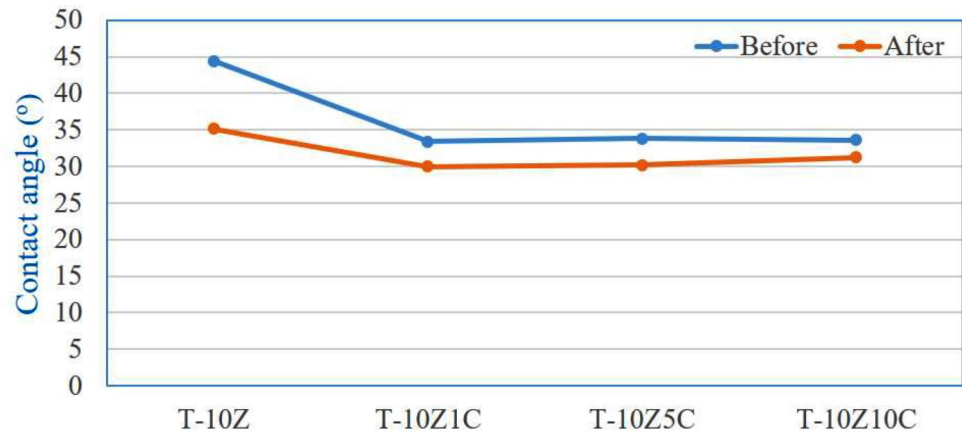
### 3.7 UV light induced contact angle alteration

Contact angle change graphs under UV radiation are given in Fig. 11. Decreased contact angles and increased hydrophilic character have been observed on all surfaces exposed to UV radiation for 60 min. Increasing the content of Cu resulted in an increase in the hydrophilic effect and a

decrease in the contact angle. Myint and colleagues previously demonstrated hydrophobic/hydrophilic switching on zinc oxide micro-textured surfaces [26]. Surface wettability is affected by its morphology, including surface roughness and micro-nanostructure, as well as the material-specific surface energy. Hydrophilic materials with a water contact angle (WCA) of less than 90 degrees can be transformed into hydrophobic materials with a WCA more than 90 degrees, and even superhydrophobic materials with a WCA exceeding 150 degrees by altering the surface structure. Das et al. have demonstrated that the water contact angle (WCA) can be altered from 104° to 135° through the straightforward adjustment of surface morphology [41].

As photo induced surface wettability conversion has been noticed on ZnO and TiO<sub>2</sub> thin films, there has been significant interest in the interaction of water droplets with nanostructured coatings made of metal oxide particles,

**Fig. 11** Changes in contact angles resulting from UV radiation



including nanorods and microrods [42]. Khranovskyy et al. demonstrated photo induced surface wettability on several ZnO nanostructures. The study examined how the size of nanostructures affects switching rate and wetness under UV illumination [43]. Han and Gao demonstrated the switchable wettability of ZnO microrods by varying WCA from 0 to 15 during UV exposure and darkness cycles [43, 44]. The study concluded that the contact angles decreased due to an increase in surface roughness, specific surface energy, and mineralogical changes resulting from Cu doping.

## 4 Conclusions

The addition of nano ZnO powder to an industrially applicable glaze led to the formation of willemite ( $\text{Zn}_2\text{SiO}_4$ ), zincite (ZnO), plagioclase crystals, with trace amounts of quartz and cristobalite. The formation of plagioclase crystals was enhanced by doping ZnO modified glazing with Cu; the maximum P/W ratio was attained with 1% Cu doping. The addition of 5% Cu improved the clarity of willemite crystals and significantly reduced the P/W ratio. Zincite phase content increases with copper doping, whereas the W to ZN ratio remains constant at all levels of doping. Increased Cu concentration from 1 to 5% made the Willemite phase more stable than the Plagioclase phase. The images from the SEM showed that the incorporation of 5 and 10% Cu enhanced the quantity of Willemite crystals. Increasing copper doping to 10% reduces the size of Plagioclase crystals and increases their number, resulting in a higher P/W ratio. Cu doping resulted in a relatively higher surface roughness value and a lower contact angle. Because surface roughness and surface chemistry are the main factors that affect the contact angle, all of the surfaces that are made have nearly the same values for surface roughness and surface energy. They are may have resulted in a higher contact angle's also all hydrophilic. A greater amount of the Willemite phase in comparison to the zincite and Plagioclase phases have resulted in a higher

contact angle. As the ZN/W ratio grew, the contact angle decreased in respect to the phase. After 60 min of UV radiation exposure, all surfaces showed reduced contact angles and enhanced hydrophilic properties.

As a result of the study, it was found that the increase in surface roughness, specific surface energy and mineralogical changes caused by Cu contribution were the main reasons for the decrease in contact angles.

**Acknowledgements** This work was supported by The Scientific and Technological Research Council of Türkiye (TÜBİTAK) [grant numbers: 222M414].

**Author contributions** Gokhan Acikbas: Supervision, Conceptualization, Methodology, Validation, Interpretation of data, Visualization, Resources, Writing - original draft; Nurcan Calis Acikbas: Interpretation of data, Revised it critically for important intellectual content, Writing-editing, Approved the version to be published; Elif Ubay: Methodology, Resources; Huseyin Karaer: Methodology, Validation.

**Funding** Open access funding provided by the Scientific and Technological Research Council of Türkiye (TÜBİTAK).

**Data availability** The data that support the findings of this study are openly available.

## Declarations

**Conflict of interest** The authors declare that they have no known competing financial interests or personal relationships that could have appeared to influence the work reported in this paper.

**Open Access** This article is licensed under a Creative Commons Attribution 4.0 International License, which permits use, sharing, adaptation, distribution and reproduction in any medium or format, as long as you give appropriate credit to the original author(s) and the source, provide a link to the Creative Commons licence, and indicate if changes were made. The images or other third party material in this article are included in the article's Creative Commons licence, unless indicated otherwise in a credit line to the material. If material is not included in the article's Creative Commons licence and your intended use is not permitted by statutory regulation or exceeds the permitted use, you will need to obtain permission directly from the copyright

holder. To view a copy of this licence, visit <http://creativecommons.org/licenses/by/4.0/>.

## References

1. L. Baraldi, M.M.E.S. Acimac, World production and consumption of ceramic tiles. *Oceania*. **56**, 1–4 (2016)
2. E. Sánchez, J. García-Ten, V. Sanz, A. Moreno, Porcelain tile: almost 30 years of steady scientific-technological evolution. *Ceram. Int.* **36**(3), 831–845 (2010)
3. M. Bondioli, R. Dinelli, M. Giovanardi, Giorgi, Functionalization of ceramic tile surface by soluble salts addition: part II. Titanium and silver addition. *J. Euro. Ceram. Soc.* **30**, 1873–1878 (2010)
4. F. Bondioli, T. Manfredini, M. Giorgi, G. Vignali, Functionalization of ceramic tile surface by soluble salts addition: part I. *J. Eur. Ceram. Soc.* **30**(1), 11–16 (2010)
5. F. Bondioli, R. Taurino, A.M. Ferrari, Functionalization of ceramic tile surface by sol–gel technique. *J. Colloid Interface Sci.* **334**(2), 195–201 (2009)
6. J.J. Reinoso, E. Enríquez, V. Fuertes, S. Liu, J. Menéndez, J.F. Fernández, The challenge of antimicrobial glazed ceramic surfaces. *Ceram. Int.* **48**(6), 7393–7404 (2022)
7. Z. Bayer Ozturk, B. Yıldız, A. Kara, Effects of alumina and white fused alumina addition on technological properties of transparent floor tile glazes. *J. Therm. Anal. Calorim.* **142**, 1215–1221 (2020)
8. A.M. Berto, Ceramic tiles: above and beyond traditional applications. *J. Eur. Ceram. Soc.* **27**(2–3), 1607–1613 (2007)
9. S.K. Fatah, M.K. Aminian, M. Bahamirian, Multifunctional superhydrophobic and cool coating surfaces of the blue ceramic nanopigments based on the heulandite zeolite. *Ceram. Int.* **48**(15), 21954–21966 (2022)
10. de S. Niederhäusern, M. Bondi, F. Bondioli, Self-cleaning and antibacteric ceramic tile surface. *Int. J. Appl. Ceram. Technol.* **10**(6), 949–956 (2013)
11. J.J. Reinoso, J.J. Romero, P. Jaquotot, M.A. Bengochea, J.F. Fernández, Copper based hydrophobic ceramic nanocoating. *J. Eur. Ceram. Soc.* **32**(2), 277–282 (2012)
12. S. Özcan, G. Açıkbaş, N.Ç. Açıkbaş, Induced superhydrophobic and antimicrobial character of zinc metal modified ceramic wall tile surfaces. *Appl. Surf. Sci.* **438**, 136–146 (2018)
13. G. Acikbas, N. Calis Acikbas, Nanoarchitectonics for polymer-ceramic hybrid coated ceramic tiles for antibacterial activity and wettability. *Appl. Phys. A* **127**, 1–11 (2021)
14. V. Golshan, F. Mirjalili, M. Fakharpour, Self-cleaning surfaces with superhydrophobicity of Ag–TiO<sub>2</sub> nanofilms on the floor ceramic tiles. *Glass Phys. Chem.* **48**(1), 35–42 (2022)
15. G. Acikbas, N. Calis Acikbas, Copper oxide-and copper-modified antibacterial ceramic surfaces. *J. Am. Ceram. Soc.* **105**(2), 873–887 (2022)
16. B.O. Bica, de J.V.S. Melo, Concrete blocks nano-modified with zinc oxide (ZnO) for photocatalytic paving: performance comparison with titanium dioxide (TiO<sub>2</sub>). *Constr. Build. Mater.* **252**, 119120 (2020)
17. H.M. Kim, D. Kim, B. Kim, Photoinduced hydrophilicity of TiO<sub>2</sub>/WO<sub>3</sub> double layer films. *Surf. Coat. Technol.* **271**, 18–21 (2015)
18. S. Qian, X. Liu, C. Ding, Effect of Si-incorporation on hydrophilicity and bioactivity of titania film. *Surf. Coat. Technol.* **229**, 156–161 (2013)
19. K. Guan, Relationship between photocatalytic activity, hydrophilicity and self-cleaning effect of TiO<sub>2</sub>/SiO<sub>2</sub> films. *Surf. Coat. Technol.* **191**(2–3), 155–160 (2005)
20. E. Rego, J. Marto, P. São Marcos, J.A. Labrincha, Decolouration of Orange II solutions by TiO<sub>2</sub> and ZnO active layers screen-printed on ceramic tiles under sunlight irradiation. *Appl. Catal. A* **355**(1–2), 109–114 (2009)
21. J. Marto, P. São Marcos, T. Trindade, J.A. Labrincha, Photocatalytic decolouration of Orange II by ZnO active layers screen-printed on ceramic tiles. *J. Hazard. Mater.* **163**(1), 36–42 (2009)
22. H.G. Carrillo, E.J. Relinque, A.M. Ramírez, M. Castellote, M.R. Pérez, Optimising processing conditions for the functionalisation of photocatalytic glazes by ZnO nanoparticle deposition. *Materiales De construcción.* **71**(344), 7 (2021)
23. J. Kim, D. Jeong, J. Choi, U. Kim, Changes in the glaze characteristics and moderate antibacterial activity of ceramic tile glazes with the addition of ZnO. *J. Asian. Ceam. Soc.* **10**(1), 241–252 (2022)
24. M.H. Lin, Y.H. Wang, C.H. Kuo, S.F. Ou, P.Z. Huang, T.Y. Song, F.Y. Fan, Hybrid ZnO/chitosan antimicrobial coatings with enhanced mechanical and bioactive properties for titanium implants. *Carbohydr. Polym.* **257**, 117639 (2021)
25. Z.L. Wang, Zinc oxide nanostructures: growth, properties and applications. *J. Phys.: Condens. Matter.* **16**(25), R829 (2004)
26. M.T.Z. Myint, N.S. Kumar, G.L. Hornyak, J. Dutta, Hydrophobic/hydrophilic switching on zinc oxide micro-textured surface. *Appl. Surf. Sci.* **264**, 344–348 (2013)
27. B. Golzad-Nonakaran, A. Habibi-Yangjeh, Photosensitization of ZnO with Ag<sub>3</sub>VO<sub>4</sub> and AgI nanoparticles: novel ternary visible-light-driven photocatalysts with highly enhanced activity. *Adv. Powder Technol.* **27**(4), 1427–1437 (2016)
28. S. Sharma, S.K. Mehta, S.K. Kansal, N doped ZnO/C-dots nano-flowers as visible light driven photocatalyst for the degradation of malachite green dye in aqueous phase. *J. Alloys Compd.* **699**, 323–333 (2017)
29. B. Subash, B. Krishnakumar, M. Swaminathan, M. Shanthi, β-Ag<sub>2</sub>S–ZnO as a novel sunshine photocatalyst for the effective degradation of RR 120 dye. *Powder Technol.* **241**, 49–59 (2013)
30. S. Harish, M. Sabarinathan, J. Archana, M. Navaneethan, S. Ponanusamy, C. Muthamizhchelvan, Y. Hayakawa, Functional properties and enhanced visible light photocatalytic performance of V<sub>3</sub>O<sub>4</sub> nanostructures decorated ZnO nanorods. *Appl. Surf. Sci.* **418**, 171–178 (2017)
31. L. Xu, Y. Zhou, Z. Wu, G. Zheng, J. He, Y. Zhou, Improved photocatalytic activity of nanocrystalline ZnO by coupling with CuO. *J. Phys. Chem. Solids.* **106**, 29–36 (2017)
32. S. Señorís, B. Sotillo, A. Urbieto, P. Fernández, Optical spectroscopy characterization of Cu doped ZnO nano-and microstructures grown by vapor-solid method. *J. Alloys Compd.* **687**, 161–167 (2016)
33. T. Bhuyan, M. Khanuja, R. Sharma, S. Patel, M.R. Reddy, S. Anand, A. Varma, A comparative study of pure and copper (Cu)-doped ZnO nanorods for antibacterial and photocatalytic applications with their mechanism of action. *J. Nanopart. Res.* **17**, 1–11 (2015)
34. A.N. Kadam, T.G. Kim, D.S. Shin, K.M. Garadkar, J. Park, Morphological evolution of Cu doped ZnO for enhancement of photocatalytic activity. *J. Alloys Compd.* **710**, 102–113 (2017)
35. C. Xia, F. Wang, C. Hu, Theoretical and experimental studies on electronic structure and optical properties of Cu-doped ZnO. *J. Alloys Compd.* **589**, 604–608 (2014)
36. Q. Ma, X. Yang, X. Lv, H. Jia, Y. Wang, Cu doped ZnO hierarchical nanostructures: morphological evolution and photocatalytic property. *J. Mater. Sci.: Mater. Electron.* **30**, 2309–2315 (2019)
37. I.A. Hassan, S. Sathasivam, S.P. Nair, C.J. Carmalt, Antimicrobial properties of copper-doped ZnO coatings under darkness and white light illumination. *ACS Omega.* **2**(8), 4556–4562 (2017)
38. F.M. Fowkes, Attractive forces at interfaces. *Industrial Eng. Chem.* **56**(12), 40–52 (1964)
39. D.K. Owens, R.C. Wendt, Estimation of the surface free energy of polymers. *J. Appl. Polym. Sci.* **13**(8), 1741–1747 (1969)



40. D.H. Kaelble, Dispersion-polar surface tension properties of organic solids. *J. Adhes.* **2**(2), 66–81 (1970)
41. S.N. Das, J.H. Choi, J.P. Kar, J.M. Myoung, Tunable and reversible surface wettability transition of vertically aligned ZnO nanorod arrays. *Appl. Surf. Sci.* **255**(16), 7319–7322 (2009)
42. R.D. Sun, A. Nakajima, A. Fujishima, T. Watanabe, K. Hashimoto, Photoinduced surface wettability conversion of ZnO and TiO<sub>2</sub> thin films. *J. Phys. Chem. B* **105**(10), 1984–1990 (2001)
43. V. Khranovskyy, T. Ekblad, R. Yakimova, L. Hultman, Surface morphology effects on the light-controlled wettability of ZnO nanostructures. *Appl. Surf. Sci.* **258**(20), 8146–8152 (2012)
44. J. Han, W. Gao, Surface wettability of nanostructured zinc oxide films. *J. Electron. Mater.* **38**, 601–608 (2009)

**Publisher's Note** Springer Nature remains neutral with regard to jurisdictional claims in published maps and institutional affiliations.